Onset of Nuclear Vaporization in ^{197}Au + ^{197}Au Collisions

M. B. Tsang, W. C. Hsi, W. G. Lynch, D. R. Bowman,* C. K. Gelbke, M. A. Lisa, and G. F. Peaslee

Department of Physics and Astronomy and National Superconducting Cyclotron Laboratory, Michigan State University, East Lansing, Michigan 48824

G. J. Kunde, M. L. Begemann-Blaich, T. Hofmann, J. Hubele, J. Kempter, P. Kreutz, W. D. Kunze, V. Lindenstruth, U. Lynen, M. Mang, W. F. J. Müller, M. Neumann, B. Ocker, C. A. Ogilvie,† J. Pochodzalla, F. Rosenberger, H. Sann, A. Schüttauf, V. Serfling, J. Stroth, W. Trautmann, A. Tucholski,‡ A. Wörner, E. Zude, and B. Zwieglinski‡

Gesellschaft für Schwerionenforschung, D-6100 Darmstadt, Germany

S. Aiello, G. Immé, V. Pappalardo, and G. Raciti

Dipartimento di Fisica Università and Istituto Nazionale di Fisica Nucleare-Catania, I95127 Catania, Italy

R. J. Charity and L. G. Sobotka

Department of Chemistry, Washington University, St. Louis, Missouri 63130

I. Iori, A. Moroni, R. Scardoni, and A. Ferrero§

Istituto di Scienze Fisiche, Universita degli Studi di Milano, I20133 Milano, Italy

W. Seidel

Forschungszentrum Rossendorf, Dresden, Germany

Th. Blaich

Institut für Kernchemie, Universität Mainz, Mainz, Germany

L. Stuttge and A. Cosmo

Centre de Recherches Nucléaires, Strasbourg, France

W. A. Friedman

Department of Physics, University of Wisconsin, Madison, Wisconsin 53706

G. Peilert

Lawrence Livermore National Laboratory, Livermore, California 94550

Multifragmentation has been measured for ^{197}Au + ^{197}Au collisions at $E/A = 100$, 250, and 400 MeV. The mean fragment multiplicity increases monotonically with the charged particle multiplicity at $E/A = 100$ MeV, but decreases for central collisions with incident energy, consistent with the onset of nuclear vaporization. Molecular dynamics calculations follow some trends but underpredict the observed fragment multiplicities. Including the statistical decay of excited residues improves the agreement for peripheral collisions but worsens it for central collisions.

PACS numbers: 25.70.Pq, 25.70.Gh

Highly excited systems can be formed during energetic nucleus-nucleus collisions, which expand due to thermal pressure [1,2] or via dynamical compression-decompression cycles [3]. For systems which expand to low densities where bulk nuclear matter is thermodynamically unstable, the growth of density fluctuations may favor multifragment disintegrations [4–6], and such disintegrations have been observed [7–12]. While definitive interpretations are premature, calculations predict that the onset of multifragmentation and the transition from multifragmentation into vaporization may be sensitive to the low density equation of state [2,13] and the liquid-gas phase transition of nuclear matter [14–17].

The incident energy dependence of multifragmentation has been recently explored for ^{36}Ar + ^{197}Au collisions between $E/A = 35$ and 110 MeV [7]. These investigations reveal large fragment multiplicities for central collisions, which increase monotonically with incident energy. Over a broader range of incident energies, however, calculations predict a maximum in the fragment multiplicity for central collisions at $E/A \approx 100$ MeV [18], and decreasing multiplicities thereafter, consistent with the onset of nuclear vaporization [4,5]. The availability of corresponding data is limited. Measurements of central ^{197}Au + ^{197}Au collisions at $E/A = 150$ and 200 MeV [8,9] displayed multifragmentation, but did not indicate the in-

cident energy dependence of the phenomenon. Measurements of multifragmentation in peripheral collisions at higher incident energies [10,11] suggested declining fragment multiplicities with decreasing impact parameters, but lacked sufficient phase space coverage to draw definitive conclusions about central collisions.

To investigate the evolution from multifragmentation towards vaporization for central ^{197}Au+^{197}Au collisions, thin 3 and 5 mg/cm^2 ^{197}Au targets were bombarded with ^{197}Au ions of $E/A = 100$, 250, and 400 MeV at the SIS facility at GSI. Three detection arrays were combined to provide an efficient 4π multifragment detection capability. At polar angles of $14.5° \leq \Theta_{lab} \leq 160°$, charged particles were detected in 215 plastic-scintillator-CsI(Tl) phoswich detectors of the Miniball/Miniwall [19]. Intermediate mass fragments (IMF's: $Z = 3$-30) that penetrated the plastic-scintillator foils of the phoswich detectors were distinguished from light particles ($Z \leq 2$); particles were further identified by element for $Z \leq 10$ and isotopically for $Z = 1$. For $25° \leq \Theta_{lab} \leq 160°$, 4 mg/cm^2 plastic-scintillator foils were used; the thresholds for particle identification in these detectors were $E_{th}/A \sim 1.5$ MeV (2.5 MeV) for $Z = 3$ ($Z = 10$) particles, respectively. For $14.5° \leq \Theta_{lab} \leq 25°$, 8 mg/cm^2 plastic foils were used; a threshold at about $E_{th}/A \sim 5$ MeV was imposed in the off-line analysis of these detectors. (Some lower energy particles were also detected but not identified.) Beam rapidity fragments with $2 \leq Z \leq 79$ were detected with the Aladin spectrometer system [20], which covered $|\Theta_{lab}| \leq 10°$ in the horizontal (bend) plane and $|\Theta_{lab}| \leq 5°$ in the vertical plane. IMF's emitted to angles between the Aladin spectrometer and the Miniball/Miniwall were detected in 84 elements of a Si-CsI(Tl) array, each consisting of 300 μm thick Si and 6 cm thick CsI(Tl) detectors, with representative thresholds of $E_{th}/A \sim 7.5$ MeV (14.5 MeV) for $Z = 3$ ($Z = 109$) particles, respectively. Fragments that penetrated through the CsI(Tl) crystals of the combined array and were not distinguished from light particles were not counted as IMF's.

Figure 1 shows the correlation between $\langle N_{IMF}\rangle$, the mean IMF multiplicity measured in the combined arrays, and N_C, the total charge particle multiplicity detected in the Miniball/Miniwall, for three incident energies. The observed dependence of $\langle N_{IMF}\rangle$ upon N_C reflects the dependence of both quantities upon the impact parameter. To allow quantitative comparisons with fragmentation models, we assumed that the charged particle multiplicity N_C depends monotonically upon the impact parameter [21],

$$\hat{b} = \frac{b}{b_{max}} = \left[\int_{N_C(b)}^{\infty} dN_C\, P(N_C)\right]^{1/2}, \quad (1)$$

and assigned a mean "reduced" impact parameter $\hat{b}$ to each data point using Eq. (1). Here, $P(N_C)$ is the probability distribution for the charged particle multiplicity for
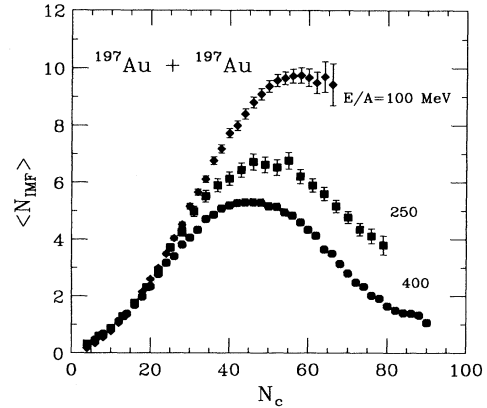

FIG. 1. Correlation between $\langle N_{IMF}\rangle$, the mean fragment multiplicity, and N_C, the multiplicity of charged particles detected in the Miniball/Miniwall. These are the measured quantities and are not corrected for the energy and angle dependent detection efficiency of the experimental apparatus.

$N_C \geq 4$, and b_{max} is the mean impact parameter with $N_C = 4$.

Figure 2 shows the mean IMF multiplicities as a function of $\hat{b}$. At $E/A = 100$ MeV, $\langle N_{IMF}\rangle$ is largest for small impact parameters, consistent with increased multifragmentation for collisions with increased compression and increased excitation energy. Contrary to the incident energy dependence observed at lower incident energies [7], however, the fragment multiplicities in central collisions
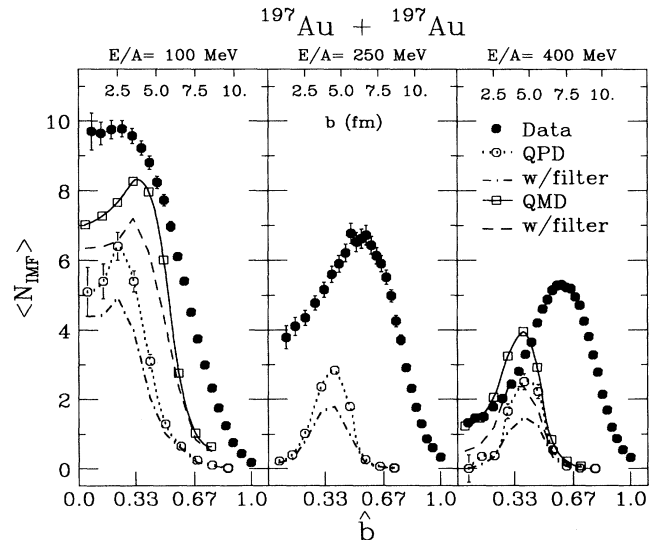

FIG. 2. The measured impact parameter dependence of the mean fragment multiplicity is shown by the solid points. The open circles and open squares depict the unfiltered predictions of the QPD and QMD models, respectively. The dash-dotted and dashed lines depict the QPD and QMD calculations, filtered through the experimental acceptance.

decrease strongly with incident energy, consistent with the onset of vaporization in systems that are too highly excited to produce significant numbers of fragments. The comparison between the data at the lowest and highest energies is most striking; multifragmentation is strongly suppressed for the overheated systems produced in central collisions at $E/A = 400$ MeV. For the more weakly excited systems produced in more peripheral collisions, multifragmentation persists, and large fragment multiplicities, e.g., $\langle N_{IMF} \rangle \approx 5$–6 for $\hat{b} \approx 0.67$ and $E/A = 400$ MeV, are observed.

Over much of the incident energy domain spanned in this Letter, both multifragmentation and collective flow have been successfully modeled for central collisions via microscopic molecular dynamics models [18,22,23]. It is interesting to explore whether such models can also describe the observed decline of multifragmentation for central collisions. The open squares in Fig. 2 are the IMF multiplicities predicted by the quantum molecular dynamics (QMD) model of Ref. [23]. The open circles in Fig. 2 are the IMF multiplicities predicted by the quasi-particle dynamics (QPD) model of Ref. [22]. Both calculations were plotted at reduced impact parameters $\hat{b}$, scaled according to the QPD calculations and the requirement that $\langle N_C \rangle = 4$ at b_{max}, dictated by Eq. (1). The actual impact parameters are given at the top of Fig. 2. Both models predict enhanced fragment multiplicities for central collisions at $E/A = 100$ MeV, but they underpredict the measured peak IMF multiplicities, and they underestimate the shift in the peak fragment multiplicity to larger impact parameters with incident energy. These discrepancies are exacerbated when the QMD and QPD calculations are correct (filtered) for the detection efficiency; filtered calculations are indicated by the dashed and dash-dotted lines in the figure.

Failures of QMD and QPD calculations to reproduce large IMF multiplicities observed at lower incident energies [7,24,25] and large impact parameters [10] have been attributed to an inadequate treatment of statistical fluctuations that lead to the decay of highly excited reaction residues [25]. Such residues are produced at $b \geq 4$ fm in the present QMD and QPD simulations, but are predicted to decay primarily by nucleon emission [23], *not by fragment emission* as predicted by statistical models [2,4,6,14,17]. The suppression of statistical fragment emission in QMD and QPD calculations is not fully understood, but it may be related to the classical heat capacities [23,26,27], the suppression of Fermi motion [23], and the neglect of quantum fluctuations within the hot residual nuclei, as modeled therein.

To illustrate such statistical decay effects, we have taken the masses and excitation energies of fragments produced in the QMD and QPD calculations as the initial conditions for statistical model calculations, using two different statistical models which both predict a multifragment decay of sufficiently hot residues at low density [2,14]. For the QMD model, the decays of all frag-

ments with $A > 4$ were calculated via the statistical multifragmentation model (SMM) of Ref. [14], which contains a "cracking" phase transition at low density. Input excitation energies and masses for the SMM calculations were taken from the QMD calculations at an elapsed reaction time of 200 fm/c. For the QPD model, the decays of bound fragments with $A > 20$ were calculated via the expanding evaporating source (EES) model of Ref. [2], which describes the evaporative decay of a hot residue expanding self-consistently under its own thermal pressure. Here, the residue properties are evaluated within 10 fm/c after the separation of the hot projectile and targetlike residues.

The open squares and circles in Fig. 3(b) are the predictions from the hybrid QMD-SMM and QPD-EES models, respectively, without correction for the detection efficiency of the experimental apparatus. The dashed curve shows the QMD-SMM predictions after the efficiency corrections for the experimental apparatus were applied. Including the statistical decay of heavy residues increases the peak values for $\langle N_{IMF} \rangle$ in both models to $\langle N_{IMF} \rangle \approx 7$–9 for $E/A = 400$ MeV and moves the peak to larger impact parameters, consistent with experimental observations. Both hybrid models underpredict the IMF multiplicity at small impact parameters. This reduction is even more evident in the QMD-SMM model predictions at $E/A = 100$ MeV; see Fig. 3(a). For such collisions, IMF's are either produced by the QMD model in insufficient quantities or are too highly excited to survive the SMM statistical decay in numbers consistent with the experimental observations.
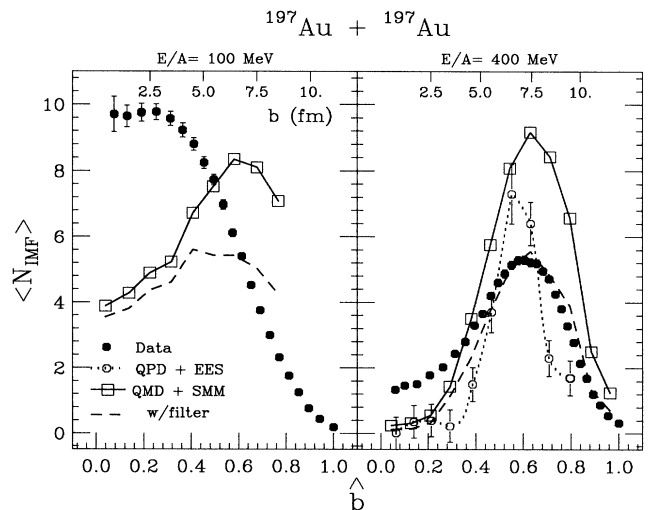

FIG. 3. Comparisons with hybrid model calculations at $E/A = 100$ and 400 MeV. The solid points depict the data. The open circles and open squares depict the unfiltered predictions of the QPD-EES and QMD-SMM models, respectively. The dashed lines depict the QMD-SMM hybrid model calculations, filtered through the experimental acceptance. The impact parameter scales are identical to those given in Fig. 2.

In summary, we have investigated ^{197}Au + ^{197}Au collisions at $E/A = 100$, 250, and 400 MeV. For central collisions at $E/A = 100$ MeV, an average number of nearly 10 intermediate mass fragments is detected, about 50% larger than the largest fragment multiplicities previously observed. The onset of nuclear vaporization with incident energy is observed; mean IMF multiplicities are reduced to less than 2 for central collisions at $E/A = 400$ MeV, and the peak IMF multiplicity is shifted to larger impact parameters. Microscopic molecular dynamics models generally underestimate the fragment yields and predict and incorrect impact parameter dependence for the IMF multiplicity at the highest incident energy. The description of peripheral collisions at $E/A = 400$ MeV can be improved by including the statistical decay of bound residues produced in the molecular dynamics simulations. Including such effects, however, worsens the agreement for central collisions.

*Present address: Chalk River Laboratories, Chalk River, Ontario, Canada K0J 1J0.
†Present address: Department of Physics, MIT, Cambridge, MA 02139.
‡Present address: Soltan Institute for Nuclear Studies, Hoza 69, 00-681 Warsaw, Poland.
§On leave from the Comision Nacional Energia Atomica, Argentina.

[1] H. Schulz et al., Phys. Lett. 147B, 17 (1984).
[2] W. A. Friedman et al., Phys. Rev. C 42, 667 (1990).
[3] H. Stöcker and W. Greiner, Phys. Rep. 137, 279 (1986), and references therein.
[4] L. P. Csernai and J. Kapusta, Phys. Rep. 131, 223 (1986), and references therein.
[5] G. Bertsch and P. J. Siemens, Phys. Lett. 126B, 9 (1983).
[6] W. G. Lynch, Annu. Rev. Nucl. Part. Sci. 37, 493 (1987), and references therein.
[7] R. T. de Souza et al., Phys. Lett. B 268, 6 (1991).
[8] K. G. R. Doss et al., Phys. Rev. Lett. 59, 2720 (1987).
[9] J. P. Alard et al., Phys. Rev. Lett. 69, 889 (1992).
[10] C. A. Ogilvie et al., Phys. Rev. Lett. 67, 1214 (1991).
[11] J. Hubele et al., Phys. Rev. C 46, R1577 (1992).
[12] K. Hagel et al., Phys. Rev. Lett. 68, 2141 (1992).
[13] E. Suraud et al., Nucl. Phys. A495, 73c (1989).
[14] J. P. Bondorf et al., Nucl. Phys. A444, 460 (1985); A. S. Botvina et al., Nucl. Phys. A475, 663 (1987).
[15] G. Sauer et al., Nucl. Phys. A264, 221 (1976).
[16] H. E. Jacqaman et al., Phys. Rev. C 27, 2782 (1983).
[17] D. H. E. Gross et al., Phys. Rev. Lett. 56, 1544 (1986).
[18] G. Peilert et al., Phys. Rev. C 39, 1402 (1989), and references therein.
[19] R. T. de Souza et al., Nucl. Instrum. Methods Phys. Res., Sect. A 295, 109 (1990); the Miniwall, a granular extension of the Miniball to forward angles, uses the readout technology of D. W. Stracener et al., Nucl. Instrum. Methods Phys. Res., Sect. A 294, 485 (1990).
[20] The ALADIN Collaboration, Report No. GSI-Nachrichten-02-89, 1988 (unpublished).
[21] L. Phair et al., Nucl. Phys. A548, 489 (1992).
[22] D. H. Boal and J. N. Glosli, Phys. Rev. C 38, 1870 (1988).
[23] G. Peilert et al., Phys. Rev. C 46, 1457 (1992).
[24] D. R. Bowman et al., Phys. Rev. Lett. 67, 1527 (1991).
[25] T. C. Sangster et al., Phys. Rev. C 46, 1404 (1992).
[26] William G. Lynch, Nucl. Phys. A545, 199c (1992).
[27] D. H. Boal et al., Phys. Rev. C 40, 601 (1989).